Research in Astronomy and Astrophysics manuscript no.
(LaTeX: Paper.tex; printed on May 23, 2022; 0:37)

Temperature Dependence of Stellar Activity Cycles

Leonid Kitchatinov

Institute of Solar-Terrestrial Physics SB RAS, Lermontov Str. 126A, 664033, Irkutsk, Russian Federation;
kit@iszf.irk.ru

Received 20xx month day; accepted 20xx month day

Abstract This paper proposes the idea that the observed dependence of stellar activity cycles on rotation rate can be a manifestation of a stronger dependence on the effective temperature. Observational evidence is recalled and theoretical arguments are given for the presence of cyclic activity in the case of sufficiently slow rotation only. Slow rotation means proximity to the observed upper bound on the rotation period of solar-type stars. This maximum rotation period depends on temperature and shortens for hotter stars. The maximum rotation period is interpreted as the minimum rotation rate for operation of a large-scale dynamo. A combined model for differential rotation and the dynamo is applied to stars of different mass rotating with a rate slightly above the threshold rate for the dynamo. Computations show shorter dynamo cycles for hotter stars. The faster rotation of hotter stars is explained by the larger amplitude of the α-effect required for their dynamo. The amplitude of the (cycling) magnetic energy in the computations is proportional to the difference between the rotation period and its upper bound for the dynamo. Stars with moderately different rotation rates can differ significantly in super-criticality of their dynamos and therefore in their magnetic activity, as observed.

Key words: dynamo — stars: activity — stars: magnetic field — stars: solar-type — stars: rotation

1 INTRODUCTION

Large-scale magnetic fields and large-scale flows in late-type stars are mutually related and both are believed to be caused by global rotation. Accordingly, many observational and theoretical studies are focused on the dependence of stellar magnetic activity and/or differential rotation on the rotation rate. This paper however suggests that magnetic activity *cycles* and differential rotation are more sensitive to another stellar parameter of the effective temperature.

In the case of differential rotation, this statement is more or less evident by now. Donahue et al. (1996) interpreted the spread in rotation periods measured in long-term chromospheric activity observations (Wilson 1968; Baliunas et al. 1995) as a manifestation of stellar differential rotation. They found an increasing trend $\Delta\Omega \propto \Omega^n$ ($n \approx 0.7$) for so-defined differential rotation ($\Delta\Omega$) with angular velocity (Ω). Zeeman-Doppler Imaging (ZDI) of young solar twin AB Doradus has however shown that the rapidly rotating star possesses about the same amount of differential rotation as the Sun (Donati & Collier Cameron 1997). It has been noted that slowly rotating stars in the sample by Donahue et al. (1996) were represented by K-stars while relative fast rotation belonged to hotter G- and F-stars (see fig.3 in their paper). This is probably because the proportionality constant in the Skumanich (1972) law $\Omega \propto t^{-1/2}$ for stellar spindown is an increasing function of temperature (Barnes 2007). Among stars of approximately the same age t, cooler stars rotate more slowly. Differential rotation dependence on rotation rate when inferred from a sample of mixed spectral types can therefore include an implicit dependence on temperature (Balona & Abedigamba 2016). The theoretical model by Kitchatinov & Rüdiger (1999) has shown a much smaller differential rotation in a K5 star compared to that of a G2 star. ZDI by Barnes et al. (2005) inferred a steep trend $\Delta\Omega \propto T_{\rm eff}^{8.92}$ with the effective temperature for rapidly rotating stars. Numerical modelling by Kitchatinov & Olemskoy (2012) predicted a moderate and not monotonic dependence on rotation rate but a strong increase of $\Delta\Omega$ with $T_{\rm eff}$.

An important problem with the dynamo theory is to define periods of stellar cycles. This paper considers the possibility that stellar activity cycles can also be more dependent on temperature than on the rate of rotation. Observations of stellar cycles were mainly focused on the dependence on rotation rate. A tendency of shorter cycles for faster rotation has been found (Noyes et al. 1984b) though with a considerable scatter and possible discontinuities in this trend (Brandenburg et al. 1998; Saar & Brandenburg 1999). Several attempts at reproducing the trend with dynamo models were undertaken with mixed success (Jouve et al. 2010; Karak et al. 2014; Hazra et al. 2019; Pipin 2021).

In Section 2, we recall observational evidence and discuss theoretical arguments for the presence of activity cycles in sufficiently slow rotating stars only. The meaning of 'slow rotation' depends on spectral type. From the standpoint of dynamo theory, rotation can be considered to be slow when it is close to the minimum rate for the dynamo. Arguments are given in Sect. 2 for an increase in this minimum rate with temperature. We apply a flux-transport solar dynamo model to slowly rotating stars of different mass and temperature to compute their magnetic cycles. Section 3 explains our method and the dynamo model. The modelling results of Sect. 4 show that the dynamo-cycles shorten with increasing temperature. This gives shorter cycles for faster rotation also, though the rotation rate is not the physical parameter that controls the cycle length in the model. Section 5 Summarises the results and concludes.

2 SHOULD CYCLIC ACTIVITY BE EXPECTED FOR RAPID ROTATORS?

The project of long-term monitoring of chromospheric activity at the Mount Wilson Observatory revealed activity cycles similar to the 11-year solar cycle on many sun-like stars (Wilson 1978; Baliunas et al. 1995). Summarising the results of the project, Baliunas et al. (1995) noted that cycles on young rapid rotators are

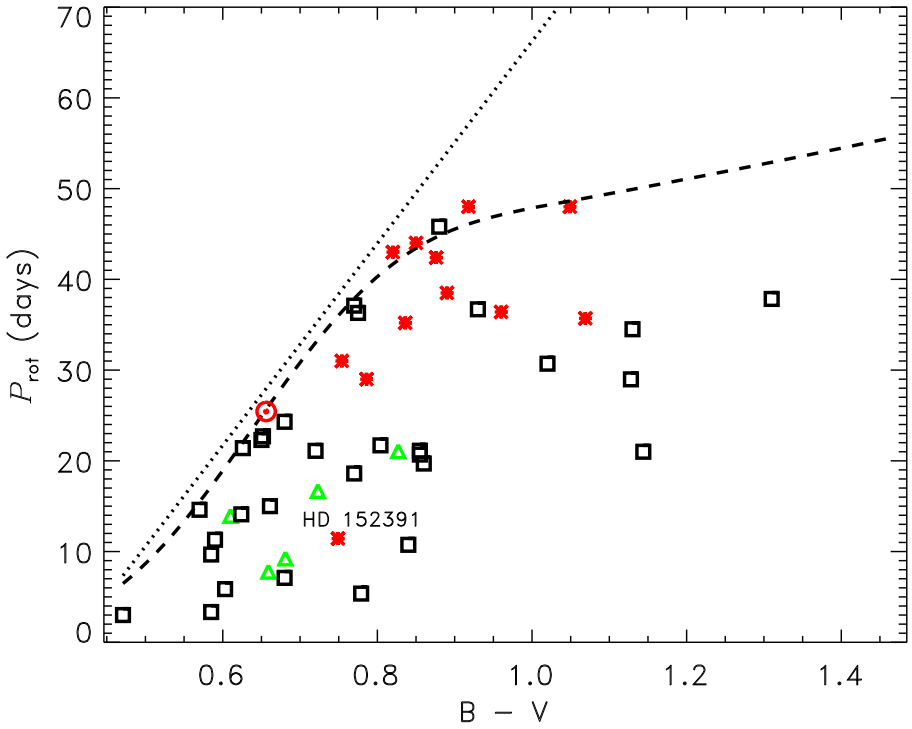

Fig. 1: Positions of the main-sequence stars showing activity cycles on the $P_{\rm rot} - (B-V)$ plane. Red symbols show stars with well-defined solar-like activity cycles. Green triangles show stars with multiple cycles and black squares - the stars with uncertain "probable" cycles. The dotted and dashed lines show the maximum rotation period $P_{\rm max}$ for stellar spindown according to Rengarajan (1984) and van Saders et al. (2019) respectively.

rare but slow rotators as old as the Sun have cycles (except for the cases of flat and low activity like the solar Mounder minimum). Recently, Boro Saikia et al. (2018) compiled a chromospheric activity catalog of Mount Wilson and more recent data on solar-type stars. Their table 4 gives stars with cyclic activity.

Figure 1 shows positions of the stars with activity cycles from the catalog by Boro Saikia et al. (2018) on the plane of the rotation period $P_{\rm rot}$ and the $B-V$ colour. Only main-sequence stars are included in the plot[1].

The rotation-colour relation is important in connection with the observational fact that the angular momentum loss essentially stops and magnetic activity is largely reduced as the rotation period increases to a maximum colour-dependent value $P_{\rm max}$ (Rengarajan 1984; Metcalfe et al. 2016; van Saders et al. 2016). The dotted line in Fig. 1 shows the linear approximation for the $P_{\rm max} - (B-V)$ relation by Rengarajan (1984). Rengarajan found this approximation for $B-V<1$. Based on a vast statistics of recent data on stellar rotation, van Saders et al. (2019) found that the $P_{\rm max} - (B-V)$ relation is well approximated by

[1] Some inaccuracies were corrected in table 4 by Boro Saikia et al. (2018) when producing Fig. 1: The color $B-V=0.594$ given in the table for HD 160343 is too small for the K3 star. It was corrected to the value of 0.971 observed (Høg et al. 2000). The HD 81809 misclassified in the table as a main-sequence star is a binary system whose active component is subgiant (Egeland 2018). Subgiants are not included in Fig. 1.

the constant value

$$\mathrm{Ro} = 2.08 \tag{1}$$

of the Rossby number $\mathrm{Ro} = P_{\rm rot}/\tau_{\rm c}$; the convective turnover time $\tau_{\rm c}$ is a function of $B-V$ colour (see eq. (4) in Noyes et al. 1984a). The $P_{\rm max}$ after Eq. (1) is shown by the dashed line in Fig. 1. Proximity to this line can quantify the meaning of 'slow rotation' for the main-sequence dwarfs.

Following Boro Saikia et al. (2018), the quality of the activity cycles is encoded by colour in Fig. 1: red symbols show well defined solar-like cycles, green triangles show stars with multiple cycles, and black squares - stars with "probable" cycles. The red symbols are close to $P_{\rm max}$-line except for HD 152391. Olspert et al. (2018) found doubly periodic activity for this star with their harmonic regression model. This may explain the position of this star in the region of green symbols in Fig. 1.

Also on physical grounds, it seems plausible to expect cyclic activity for slow rotators only.

Stellar spindown is caused by angular momentum loss for magnetically coupled wind. Large-scale magnetic fields are of key importance for this process. The fields ensure that the wind plasma does not loose contact with the parent star on the photosphere but co-rotates with the star up to a distance that is large compared to the stellar radius. In this way, the field makes a long arm for application of the spindown brake (Kraft 1967). The field is produced by the large-scale dynamo. The $P_{\rm max}$ in Fig. 1 can therefore be interpreted as the maximum rotation period for operation of the large-scale dynamo (Cameron & Schüssler 2017; Kitchatinov & Nepomnyashchikh 2017b).

Hydromagnetic dynamos of any kind can be understood as the *instability* of conducting fluids to magnetic disturbances. Only if whatever small but finite seed field is present, can a dynamo-instability amplify and support the field. Similar to all other instabilities, dynamo-instability has dimensionless governing parameters and onset when the parameters exceed a certain threshold value. The empirical Eq. (1) can be seen as the normalised rotation rate for the onset of large-scale stellar dynamos. The red symbols of Fig. 1 close to the $P_{\rm max}$-line represent slightly supercritical cyclic dynamos.

Various instabilities of fluid dynamics behave similarly in dependence on their governing parameters. For slightly supercritical parameters, new steady (change of stability) or oscillatory (overstability) states are normally realised (Chandrasekhar 1961). In a highly supercritical case, instabilities change - as a rule - to a turbulent regime possibly with an intermediate stage of multi-periodic dynamics (see, e.g., Landau & Lifshitz 1987). If large-scale dynamo instability is not an exception to this rule, some kind of dynamo turbulence with non-cyclic activity should be expected for the highly supercritical regime of rapid rotation.

The expectation is hard to test with computations. This would require fully nonlinear and highly supercritical dynamo models lacking at the moment. The strongly nonlinear dynamo regime in rapid rotators is in particular indicated by their observed large torsional oscillations (Collier Cameron & Donati 2002). Changes to turbulence usually proceed via break of symmetry of slightly supercritical regimes. An adequate dynamo model has to be nonlinear and non-axisymmetric.

Lacking such a dynamo model, we restrict our computations to slightly supercritical cyclic dynamos. A solar-type dynamo model is applied to stars of different mass and rotation period close to $P_{\rm max}$ of Fig. 1. The

computed cycle period is shorter for hotter stars. As the $P_{\max}$ decreases with temperature, the temperature dependence shows at least qualitative agreement with the observed shorter cycles for faster rotation.

3 MODEL AND METHOD

3.1 Combined model of differential rotation and dynamo

We apply a joint model of dynamo and differential rotation by Kitchatinov & Nepomnyashchikh (2017a,b) to stars of different mass $0.7 \leq M/M_\odot \leq 1.2$ and rotation period close to $P_{\max}$ of Eq. (1). Differential rotation and meridional flow for dynamo computations are supplied by an axisymmetric hydrodynamical mean-field model. The model differs from that of Kitchatinov & Olemskoy (2011) only in a modification of the mixing length ℓ: the mixing length of its standard definition $\ell_0 = \alpha_{MLT} H_{\rm p}$ ($H_{\rm p}$ is the pressure scale height) is now reduced near the inner boundary $r_{\rm i}$ of the convection zone so that it can exceed the distance to the boundary only slightly:

$$\ell = \ell_{\min} + \frac{1}{2}\left(\ell_0 - \ell_{\min}\right)\left[1 + \mathrm{erf}\left(\frac{r/r_{\rm i} - x_\ell}{d}\right)\right]. \tag{2}$$

In this equation, $\ell_{\min} = 0.01R$ equals one percent of the stellar radius, erf is the error function, and other parameters will be specified later. Our differential rotation model differs from other mean-filed formulations in that it does not prescribe the eddy transport coefficients but computes them. The eddy viscosity in particular is defined by the equation

$$\nu_{\rm T} = -\frac{\tau \ell g}{15 c_{\rm p}} \frac{\partial S}{\partial r}, \tag{3}$$

where g is gravity, τ is the (position dependent) convective turnover time, $c_{\rm p}$ is the specific heat capacity at constant pressure. The specific entropy S in Eq. (3) is a dependent variable of the model. The entropy is controlled by the (nonlinear) heat transport equation that is one of three equations of the model (the other two being the equations for the meridional flow and angular velocity). Recently Jermyn et al. (2018) discussed the performance of this closure method in the convective turbulence theory.

We avoid repeating other details of the differential rotation model all of which can be found elsewhere (Kitchatinov & Olemskoy 2011, 2012).

Our dynamo model is a particular version of the flux-transport models pioneered by Choudhuri et al. (1995) and Durney (1995). The models' name reflects the importance of magnetic field advection by the meridional flow. The flux-transport models with the α-effect of Babcock-Leighton (BL) type agree closely with solar observations (Jiang et al. 2013; Charbonneau 2020).

Our dynamo model is formulated for a spherical layer of a stellar convection zone. The standard spherical coordinate system (r, θ, ϕ) with the rotation axis as the polar axis is used. The formulation assumes axial symmetry of the mean magnetic field

$$\boldsymbol{B} = \boldsymbol{e}_\phi B + \boldsymbol{\nabla} \times \left(\boldsymbol{e}_\phi \frac{A}{r \sin\theta}\right) \tag{4}$$

and flow

$$\boldsymbol{V} = \boldsymbol{e}_\phi r \sin\theta\, \Omega + \rho^{-1} \boldsymbol{\nabla} \times \left(\boldsymbol{e}_\phi \frac{\psi}{r \sin\theta}\right). \tag{5}$$

In these equations, B is the toroidal magnetic field, A is the poloidal field potential, Ω is the angular velocity, ψ is the stream function for the meridional flow, and ρ is density.

Two joint dynamo equations for the poloidal and toroidal magnetic fields read

$$\frac{\partial A}{\partial t} = \frac{1}{\rho r^2 \sin\theta}\left(\frac{\partial\psi}{\partial r}\frac{\partial A}{\partial\theta} - \frac{\partial\psi}{\partial\theta}\frac{\partial A}{\partial r}\right) + r\sin\theta\,\mathcal{E}_\phi\,, \tag{6}$$

$$\frac{\partial B}{\partial t} = \frac{1}{\rho r^2}\frac{\partial\psi}{\partial r}\frac{\partial}{\partial\theta}\left(\frac{B}{\sin\theta}\right) - \frac{1}{r\sin\theta}\frac{\partial\psi}{\partial\theta}\frac{\partial}{\partial r}\left(\frac{B}{\rho r}\right) + \frac{1}{r}\left(\frac{\partial\Omega}{\partial r}\frac{\partial A}{\partial\theta} - \frac{\partial\Omega}{\partial\theta}\frac{\partial A}{\partial r} + \frac{\partial(r\mathcal{E}_\theta)}{\partial r} - \frac{\partial\mathcal{E}_r}{\partial\theta}\right)\,, \tag{7}$$

where $\boldsymbol{\mathcal{E}} = \langle \boldsymbol{u}\times\boldsymbol{b}\rangle$ is the mean electromotive force (EMF, see Krause & Rädler 1980), which results from a correlated action of fluctuating velocities $\boldsymbol{u}$ and magnetic fields $\boldsymbol{b}$ and includes all the dynamo-relevant effects of convective turbulence.

Expression for the EMF can be rather complicated (Pipin 2008). Some simplification can be achieved by splitting the EMF in three parts,

$$\boldsymbol{\mathcal{E}} = \boldsymbol{\mathcal{E}}^\alpha + \boldsymbol{\mathcal{E}}^{\rm diff} + \boldsymbol{\mathcal{E}}^{\rm dia}, \tag{8}$$

responsible for the α-effect, eddy diffusion, and diamagnetic pumping respectively.

Toroidal field generation by the α-effect is neglected in the $\alpha\Omega$-dynamo. Nonlocal α-effect of BL type is prescribed in the poloidal field equation (6)

$$\mathcal{E}^\alpha_\phi = \frac{\alpha\, B(r_{\rm i},\theta)}{1+(B(r_{\rm i},\theta)/B_0)^2}\cos\theta\sin^{n_\alpha}\theta\,\phi_\alpha(r/r_{\rm e}), \tag{9}$$

where the function

$$\phi_\alpha(r/r_{\rm e}) = \frac{1}{2}\left[1+{\rm erf}\left((r/r_{\rm e}+2.5h_\alpha-1)/h_\alpha\right)\right], \tag{10}$$

with $h_\alpha = 0.02$ peaks near the external boundary $r_{\rm e} = 0.97R$. This boundary is placed shortly below the stellar surface to exclude the near-surface layer of steep stratification that is difficult to include in the differential rotation model. The α-effect of Eq. (9) describes generation of the poloidal field near the surface from the bottom toroidal field. The large value of $n_\alpha = 7$ used in the model implies that the magnetic flux-tubes whose rise to the surface produces the α-effect are formed at low latitudes (Kitchatinov 2020). The value $B_0 = 10^4$ G of the α-effect quenching parameter in Eq. (9) gives reasonable results for the Sun (Kitchatinov & Nepomnyashchikh 2017a). This value was used for the star of one solar mass. For other masses, the parameter was re-scaled in proportion to the square root of density at the inner boundary, $B_0 = 10^4\sqrt{\rho_{\rm i}(M)/\rho_{\rm i}(1M_\odot)}$ G, to reflect the scaling of flux-tube rise velocity with the Alfven velocity (D'Silva & Choudhuri 1993).

Diffusive part of the EMF of our model reads

$$\boldsymbol{\mathcal{E}}^{\rm diff} = -\eta\boldsymbol{\nabla}\times\boldsymbol{B} - \eta_\parallel\hat{\boldsymbol{\Omega}}\times\left(\hat{\boldsymbol{\Omega}}\cdot\boldsymbol{\nabla}\right)\boldsymbol{B}, \tag{11}$$

where $\hat{\boldsymbol{\Omega}} = \boldsymbol{\Omega}/\Omega$ is the unit vector along the rotation axis. Magnetic diffusivity of Eq. (11) is anisotropic: the diffusivity η for a direction normal to the rotation axis is smaller than the diffusivity $\eta+\eta_\parallel$ along this axis. The anisotropy is caused by rotation,

$$\eta = \eta_{\rm T}\phi(\Omega^*),\quad \eta_\parallel = \eta_{\rm T}\phi_\parallel(\Omega^*). \tag{12}$$

The functions $\phi(\Omega^*)$ and $\phi_\parallel(\Omega)$ of the Coriolis number

$$\Omega^* = 2\tau\Omega \tag{13}$$

are given in Kitchatinov et al. (1994). The rotationally induced anisotropy is important for the differential rotation model. Only with account for anisotropy of the eddy heat transport, can the helioseismological rotation law be reproduced (Rüdiger et al. 2013). We include the diffusion anisotropy in the dynamo model for consistency and for its better performance (Pipin et al. 2012).

The diamagnetic pumping results from inhomogeneity of the turbulence intensity (Krause & Rädler 1980). Our dynamo model employs the anisotropic pumping effect for rotating fluids as it was derived by Kitchatinov & Nepomnyashchikh (2016),

$$\boldsymbol{\mathcal{E}}^{\rm dia} = -(\boldsymbol{\nabla}\tilde{\eta}) \times \boldsymbol{B} + (\boldsymbol{\nabla}\eta_\parallel) \times \hat{\boldsymbol{\Omega}}(\hat{\boldsymbol{\Omega}} \cdot \boldsymbol{B}) \,, \tag{14}$$

with another diffusivity coefficient

$$\tilde{\eta} = \eta_{\rm T}\phi_1(\Omega^*). \tag{15}$$

Allowance for the pumping effect generally improves the solar dynamo models (Guerrero & de Gouveia Dal Pino 2008; Karak & Cameron 2016; Zhang & Jiang 2022).

Magnetic eddy diffusivity $\eta_{\rm T}$ can be estimated using the computed eddy viscosity of Eq. (3), $\eta_{\rm T} = \nu_{\rm T}/{\rm Pm}$, where Pm is the magnetic Prandtl number. The problem however is that our differential rotation model uses local mixing-length approximation and does not include the low diffusivity layer of overshoot convection that is important for the dynamo. We reduce the diffusivity near the inner boundary to model the layer:

$$\eta_{\rm T} = \frac{1}{\rm Pm}\left[\nu_{\rm i} + \frac{1}{2}(\nu_{\rm T} - \nu_{\rm i})\left(1 + {\rm erf}\left(\frac{r/r_{\rm i} - x_\eta}{d}\right)\right)\right], \tag{16}$$

where $\nu_{\rm i} = 10^{-4}\nu_{\rm max}$ ($\nu_{\rm max}$ is the maximum value of $\nu_{\rm T}$ within the convection zone, Pm = 3 in all computations of this paper. Parameters in the Eqs. (2) and (16) for the star of $1M_\odot$ are taken to be $x_\ell = 1.01,\ d = 0.025,\ x_\eta = 1.1$.

Figure 2 shows depth profiles of the diffusivity coefficients of Eqs. (11) and (15) for the $1M_\odot$ star. The large (but realistic, Cameron & Schüssler 2016) diffusivity of this Figure can result in too short dynamo-cycles. Cycle periods of about 10 yr in our model are due to the downward diamagnetic pumping that transports the magnetic field into the near-bottom layer of low diffusion.

The $\eta_\parallel$ coefficient decreases towards the surface in Fig. 2. This is because the depth-dependent Coriolis number of Eq. (13) decreases towards the surface leading to a smaller rotation-induces diffusion anisotropy.

The parameter values $x_\ell = 1.01,\ d = 0.025,\ x_\eta = 1.1$ were formerly applied to stars of various mass (Kitchatinov & Nepomnyashchikh 2017b). It has been realized since then that the near bottom layer of small diffusion occupies a larger part of the convection zone in stars of larger mass in this case (a half of the thin convection zone of the $1.2M_\odot$ star). To avoid such a non-physical prescription, we re-scale the parameters so that all the characteristic scales constitute the same fractions of the convection zone thickness in stars of different mass:

$$d = 0.0745\left(\frac{r_{\rm e}}{r_{\rm i}} - 1\right), \quad x_\ell = 0.03\frac{r_{\rm e}}{r_{\rm i}} + 0.97, \quad x_\eta = 0.3\frac{r_{\rm e}}{r_{\rm i}} + 0.7. \tag{17}$$

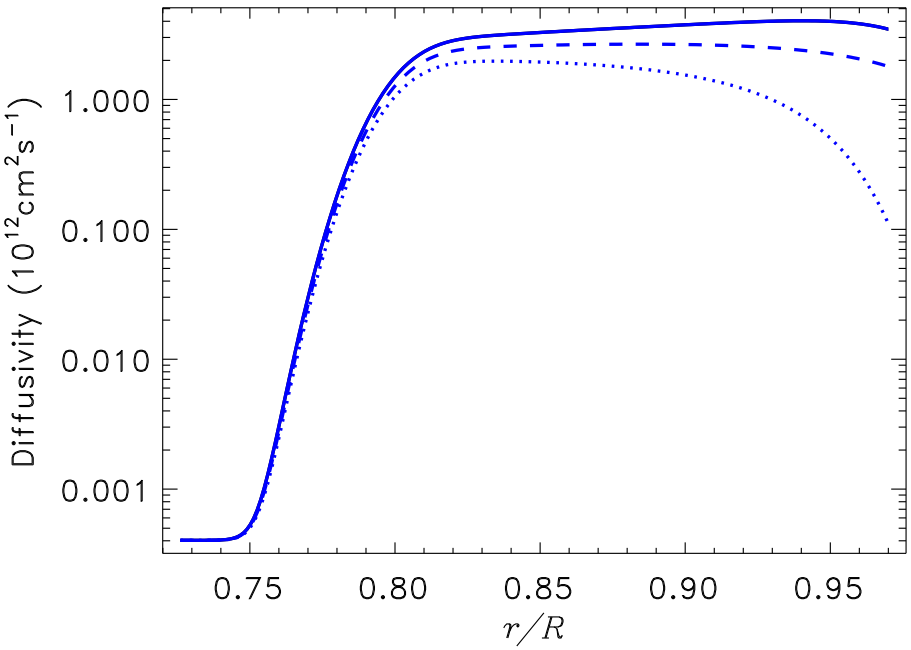

Fig. 2: Depth profiles of the diffusion coefficients η (full line), $\eta_\parallel$ (dotted) and $\tilde{\eta}$ (dashed) for a star of $1M_\odot$ rotating with a period of 23.5 days.

With this prescription, Fig. 2 looks almost the same for stars of all considered mass except for the varying minimum value of r/R in the plot. Some difference in the results of this paper with Kitchatinov & Nepomnyashchikh (2017b) is explained by the different prescription for the parameters of the Eq.(17) and in the definition of $P_{\rm max}$ by Eq. (1) which was not yet awared of in 2017.

The dynamo model solves numerically the initial value problem for dynamo equations (7) with a perfect conductor boundary condition imposed on the bottom and vertical field condition on the top. The initial condition prescribes the zero toroidal field and the potential

$$A_0(r,\theta)=\frac{B_N(r-r_{\rm i})(2r_{\rm e}-r_{\rm i}-r)}{4(1-r_{\rm i}/r_{\rm e})^2}[1-p+(1+p)\cos\theta]\sin^2\theta \qquad (18)$$

for the poloidal field, where B_N is the field strength on the northern pole and $-1\le p\le 1$ is the parity index ($p=1$ means a quadrupolar equator-symmetric initial field and $p=-1$ is for a dipolar antisymmetric field). Starting from the initial condition of mixed parity, the dynamo code was run for one thousand years simulation time. This preliminary run suffices for the dynamo to converge to a periodic oscillation, for which the cycle period and other results of Sect. 4 were obtained. If the initial condition (18) had a certain parity ($p=\pm1$), the numerical solution cannot depart from this parity. The runs with so-prescribed parity helped to compute the threshold amplitude $\alpha_{\rm c}$ of the α-effect of Eq. (9) for the onset of dynamo-instability for dipolar ($\alpha_{\rm c}^{\rm d}$) and quadrupolar ($\alpha_{\rm c}^{\rm q}$) fields.

3.2 Estimating $P_{\rm rot}$ and structure of stars

Computations of differential rotation and dynamo require the structure and rotation rate of a star to be specified.

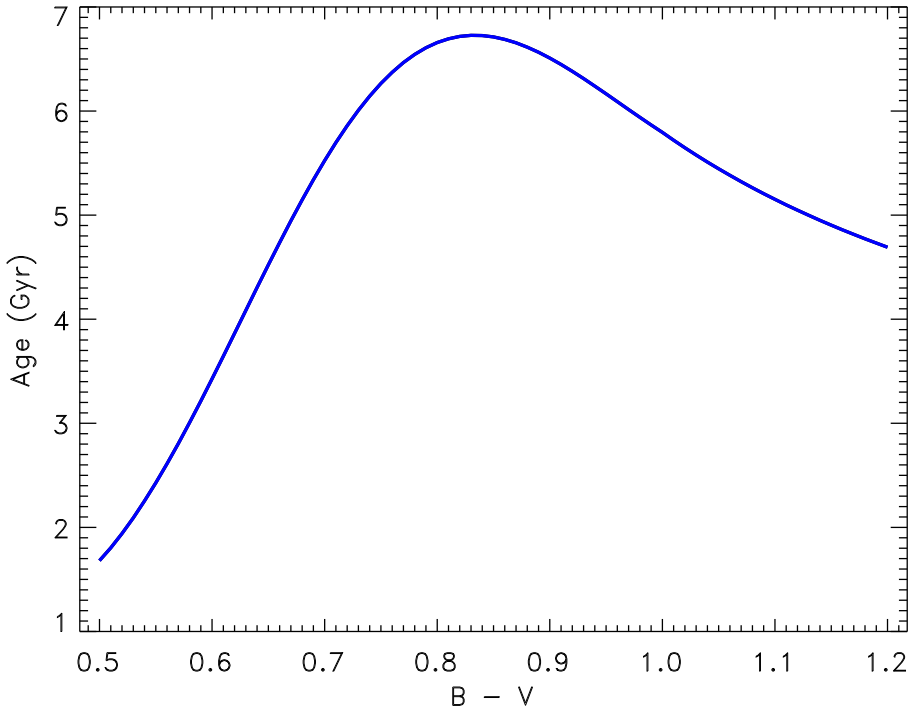

Fig. 3: Stellar age of the maximum rotation period $P_{\rm max}$ as the function of $B-V$ colour estimated with Eq. (20).

We use the gyrochronology relation by Barnes (2007)

$$P_{\rm rot} = at^n\,(B-V\ -\ 0.4)^b\ {\rm d}, \tag{19}$$

relating the age t (in Myr) and $B-V$ colour of a star to the rotation period. The parameter values of $a=0.77,\ n=0.512,\ b=0.6$ within their uncertainty range reproduce closely the case with the Sun.

Gyrochronology is believed to overestimate the rotation period after the rotation slows down to the minimum rate of Eq. (1) (van Saders et al. 2016, 2019). Stellar structure varies slowly at the age when it happens. We therefore assume that the relation (19) applies up to the age when the maximum rotation period of Eq. (1) is attained. This age can be roughly estimated from the reversed Eq. (19):

$$t = \left[\frac{2.08\ \tau_{\rm c}}{a(B-V\ -\ 0.4)^b}\right]^{1/n}. \tag{20}$$

Figure 3 shows the age of Eq. (20) as function of colour.This age of the large-scale dynamo termination does not decrease monotonously with increasing temperature.

The *EZ* code by Paxton (2004) was used to define the evolutionary sequence of structure models for a star of given mass and metallicity $Z=0.02$. The colour-temperature relation and the interpolation code by VandenBerg & Clem (2003) was used to estimate the $B-V$ color corresponding to the structure models. The rotation period of Eq.(19) was then compared with the $P_{\rm max}$ of Eq. (1). The structure model with the closest values of these two rotation periods is assumed to correspond to the star that arrived on the dashed line of Fig. 1. The Sun is almost on this line. The solar dynamo was estimated to be about 10% supercritical in the sense of the amplitude α of the α-effect of Eq. (9). The differential rotation of the stars of different

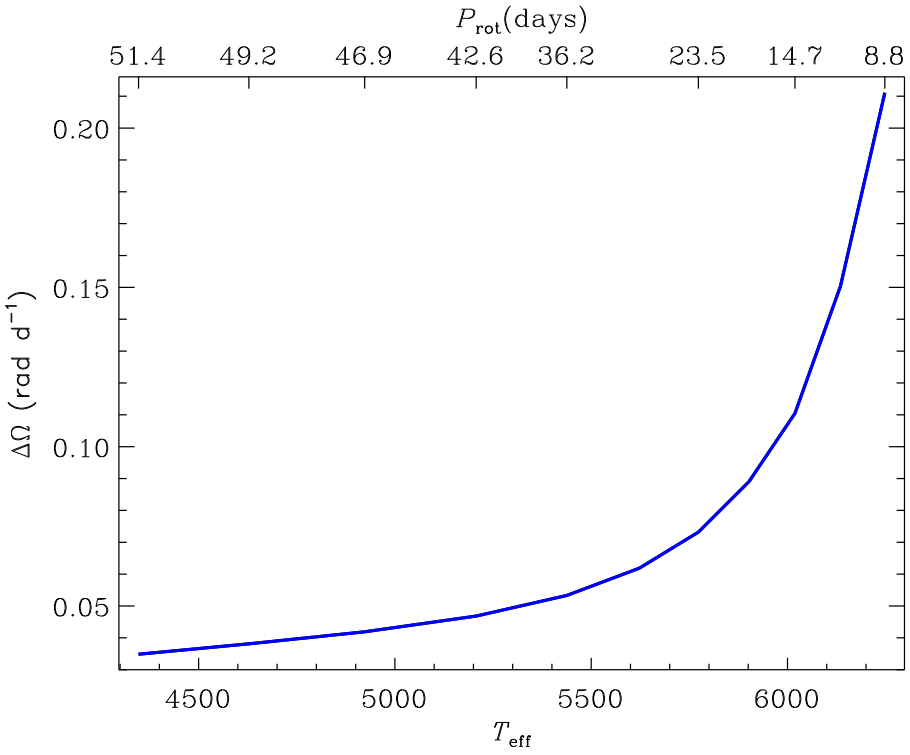

Fig. 4: Difference in rotation rates between equator and pole as the function of temperature. The scale on the top shows the rotation period corresponding to the dashed line in Fig. 1.

mass which 'arrived on the dashed line' of Fig. 1 was computed and then used in the simulations of their 10% supercritical dynamos as explained at the end of Sect. 3.1.

The computations cover the mass range from $0.7M_\odot$ to $1.2M_\odot$ with increment of $0.05M_\odot$.

4 RESULTS AND DISCUSSION

All computations show solar-type differential rotation with faster equatorial rotation. Figure 4 shows the surface equator-to-pole difference in rotation rate in dependence on the effective temperature. Hotter stars have larger differential rotation. As the hotter stars rotate faster, this Figure also means an increase in the differential rotation with rotation rate. Figure 4 is a slow rotation counterpart of fig. 10 by Kitchatinov & Olemskoy (2011).

Figure 5 shows a similar plot for the period of computed dynamo cycles. These are the periods of energy oscillation (half-periods of the sign-changing magnetic cycles). Dynamo computations predict shorter cycles for hotter stars. This temperature trend also implies a shorter cycle for faster rotation. Similar to the differential rotation, the observed decrease in activity cycle duration with rotation rate can be at least partly explained by its temperature dependence.

The difference with the differential rotation however is that the theoretical dependence of cycle period on rotation rate for fixed temperature is uncertain and may not be weak. Non-kinematic dynamo models are required to study this dependence. Consideration of Sect. 2 suggests that activity of rapidly rotating young stars is not cyclic. Katsova et al. (2015) estimated that the Sun formed its activity cycle at the age of 1 to 2

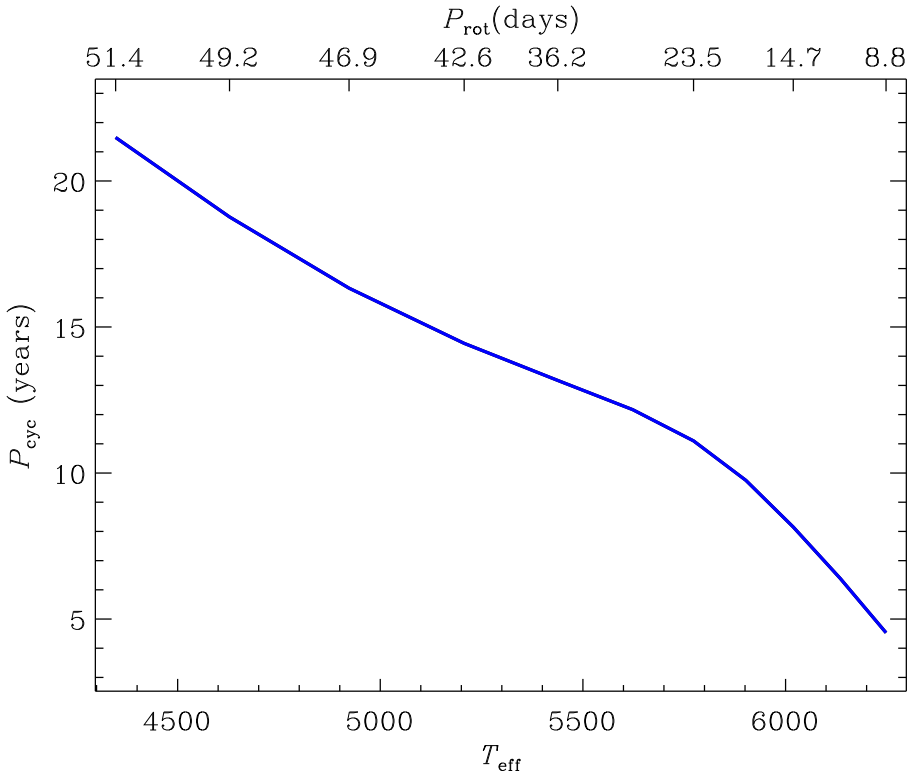

Fig. 5: Periods of the computed dynamo-cycles as the function of temperature. Similar to Fig. 4, the scale on the top shows the corresponding rotation period.

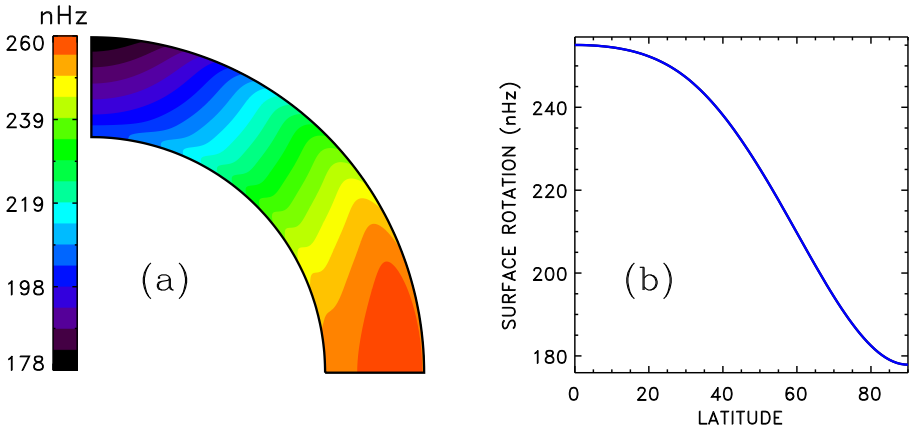

Fig. 6: Differential rotation of the $0.8M_\odot$ star. (a) Rotation rate isolines in the NW quadrant of the meridional cross-section of the convection zone. (b) Latitudinal profile of the surface rotation rate.

Gyr. This means about two times faster rotation compared to its present rate. Red symbols in Fig. 1 are not very close to the dashed line of $P_{\rm max}$.

We consider next the differential rotation and dynamo for two cases of stellar mass smaller and larger compared to the Sun. The consideration shows that equatorial symmetry of the dominant dynamo mode does also depend on temperature.

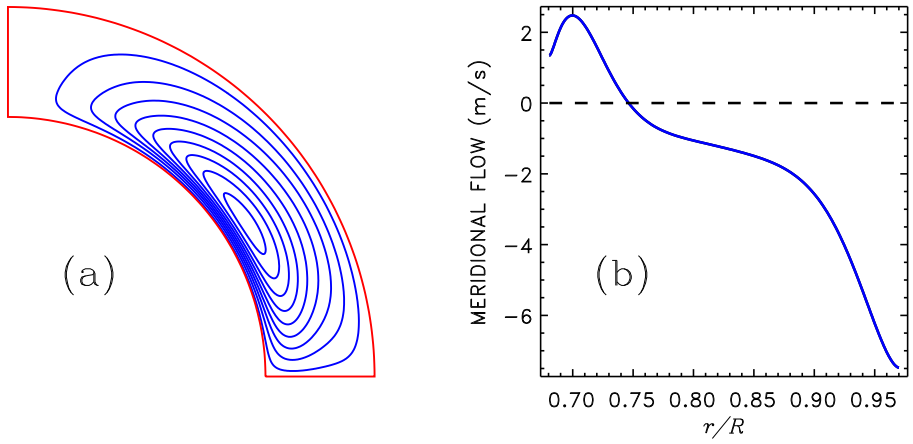

Fig. 7: Meridional flow in the $0.8M_\odot$ star. (a) Stream lines of the flow. (b) Variation of the meridional velocity with radius at the 45° latitude. Positive velocity means equator-ward flow.

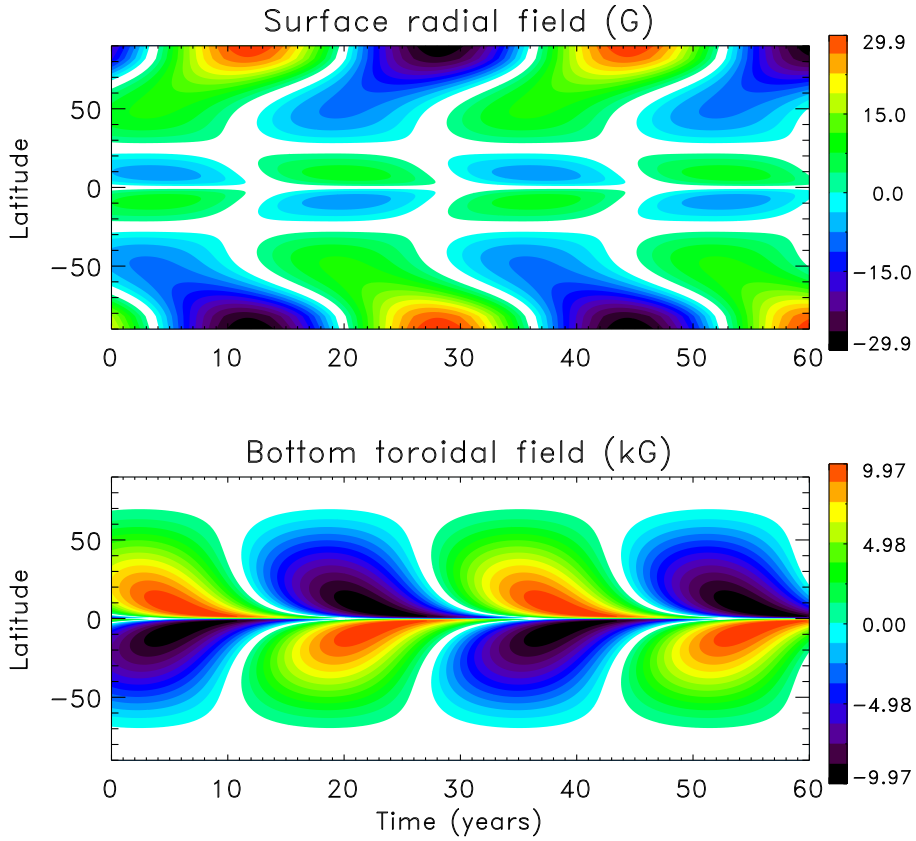

Fig. 8: Time-latitude diagrams of the dynamo model for $0.8M_\odot$ star. Surface radial field and the bottom toroidal field are shown in the top and bottom panels respectively.

Figures 6 to 8 show the differential rotation, meridional flow and magnetic time-latitude diagram computed for the $0.8M_\odot$ star. Similar to the Sun, dipolar dynamo mode dominates in this case. The dynamo arrived at dipolar parity from a mixed-parity initial state of Eq. (18).

Computations for the high mass end of the mass range concerned show dynamo convergence to the mixed parity solution. Figures 9 to 11 show the differential rotation, meridional flow and field diagram

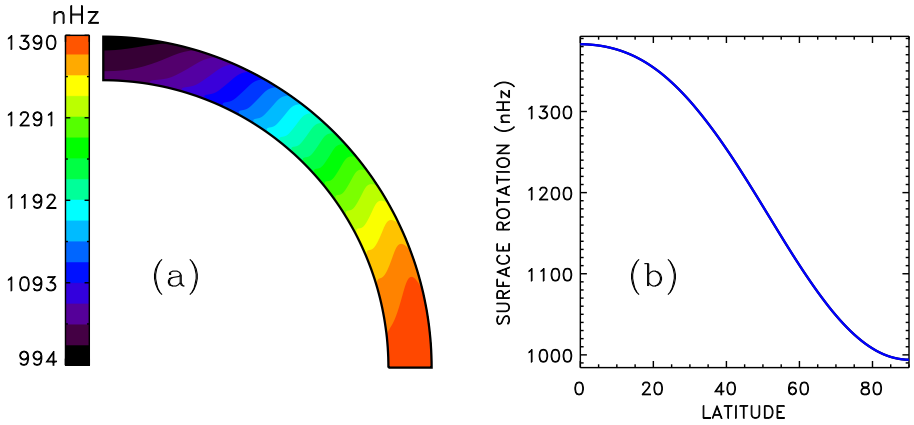

Fig. 9: Differential rotation of $1.2M_\odot$ star. (a) Rotation rate isolines. (b) Latitudinal profile of the surface rotation rate.

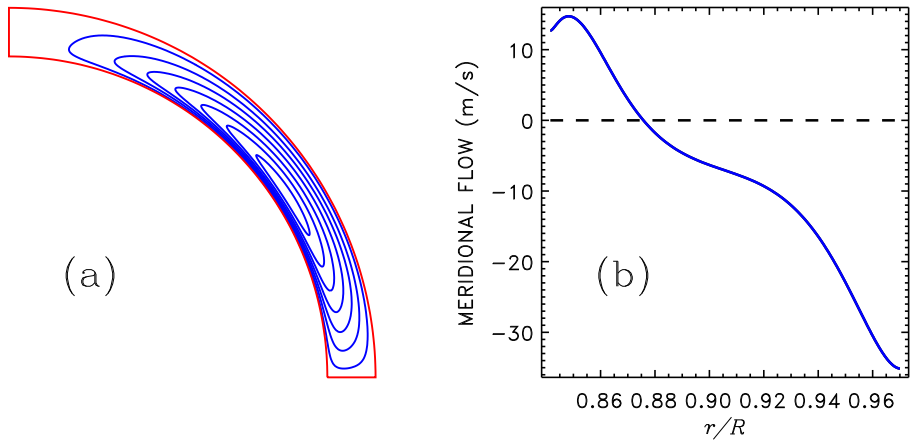

Fig. 10: Meridional flow in the $1.2M_\odot$ star. (a) Stream lines of the flow. (b) Depth profile of the meridional velocity at the 45° latitude. Positive velocity means equator-ward flow.

computed for the $1.2M_\odot$ star. In this case, rotation is faster but magnetic fields are weaker compared to the $0.8M_\odot$ star. The field diagram of Fig. 11 shows mixed equatorial symmetry. Convergence to a certain symmetry requires a certain link between the northern and southern hemispheres. The hemispheric link weakens with decreasing thickness of the convection zone in stars of larger mass.

Another manifestation of the weaker hemispheric link in the thin convection zones of relatively massive stars is the almost equal threshold amplitudes $\alpha_{\rm c}^{\rm d}$ and $\alpha_{\rm c}^{\rm q}$ for generation of dipolar and quadrupolar fields in Fig. 12. The $\alpha_{\rm c}$ of this Figure increase with temperature. A larger $\alpha_{\rm c}$ needs faster rotation. This can explain the shorter $P_{\rm max}$ for more massive stars (smaller $B-V$) in Fig. 1. Further increase in $\alpha_{\rm c}$ for $M > 1.2M_\odot$ may eventually mean that even $P_{\rm rot} \sim 1\,{\rm d}$ of *ZAMS* stars does not suffice for a dynamo. Based on observations, Durney & Latour (1978) concluded that stars of spectral type earlier than F6 do not support large-scale dynamos.

The α-effect in our computations is 10% supercritical, $\alpha = 1.1\,\alpha_{\rm c}$. Computations with other slightly supercritical α show that the amplitude B of magnetic cycles is proportional to the square root of the supercriticality, $B \propto (\alpha - \alpha_{\rm c})^{1/2}$. This relation holds not only for the dynamo-instability of this paper, but is a

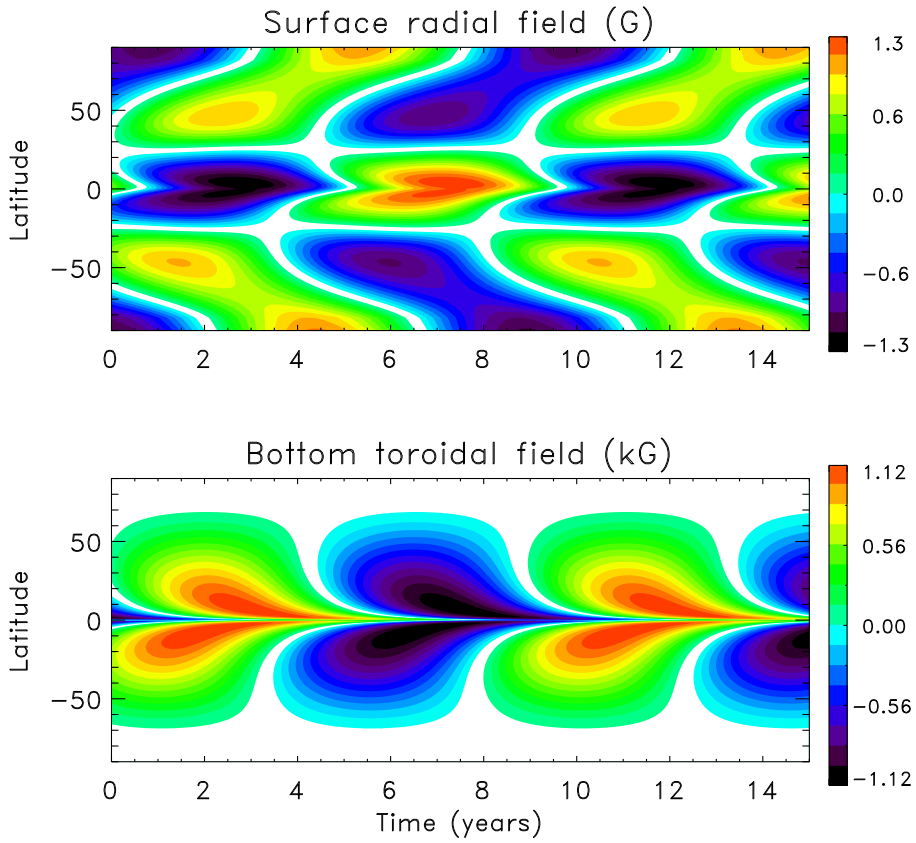

Fig. 11: Time-latitude diagrams of the dynamo model for $1.2M_\odot$ star. Surface radial field and the bottom toroidal field are shown in the top and bottom panels respectively.

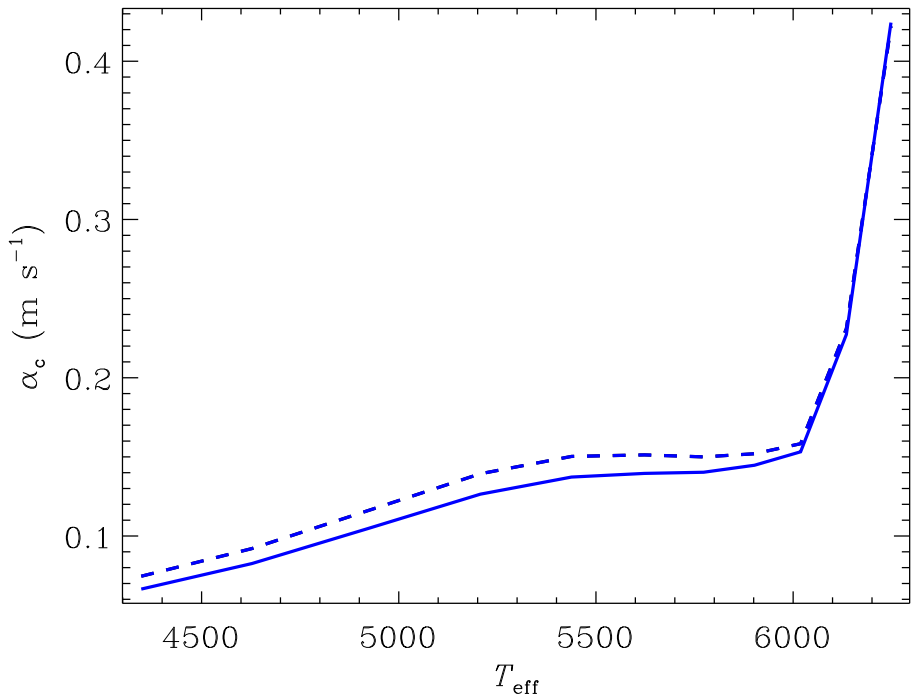

Fig. 12: Marginal amplitude α_c of the α-effect for generation of dipolar (full line) and quadrupolar (dashed) magnetic fields as the function of temperature.

general rule for weakly nonlinear instabilities (cf. eq. (26.10) in Landau & Lifshitz 1987)[2]. The relation can be reformulated in terms of the rotation rate,

$$B \propto (P_{\rm max} - P_{\rm rot})^{1/2}\,, \tag{21}$$

and possibly explain why the Sun is observed to be less active than other stars of comparable effective temperature and rotation rate (Reinhold et al. 2020; Zhang et al. 2020). According to Eq. (21), what matters for magnetic activity is not the value of the rotation rate but the amount of excess by the rate above its marginal value for dynamo. The derivative of Eq. (21) on $P_{\rm rot}$ is infinite at $P_{\rm rot} = P_{\rm max}$. Stars with close rotation rates can differ considerably in super-criticality of their dynamos.

The ratio of the cycle period to the time of advection by the meridional flow, $P_{\rm cyc}V_{\rm bot}/r_{\rm i}$, varies little to remain between the values of 3 and 4 in our computations; $V_{\rm bot}$ is the near-bottom maximum value of the meridional flow velocity (see Figs 7b and 10b). This means that the computations belong to the flux-transport dynamo regime.

A preliminary run of one thousand years starting from the mixed-parity initial state of Eq. (18) did not converge to a certain equatorial symmetry for $1.2M_\odot$ star though $\alpha_{\rm c}^{\rm q}$ is slightly smaller than $\alpha_{\rm c}^{\rm d}$ in this case (Fig. 11). We did not extend the run further for the following reason. Our computations do not include fluctuations in dynamo parameters, which are most probably present in stars. The equator-asymmetric fluctuations couple the dipolar and quadrupolar dynamo modes so that the amplitudes of these modes vary irregularly on a time scale comparable to the cycle period (Schüssler & Cameron 2018; Kitchatinov & Khlystova 2021). The amplitudes are expected to be comparable for almost equal super-criticality of the two modes. This will result in irregularly varying north-south asymmetry in activity of a star. Observational detection of an activity cycle may be difficult in this case if the inclination angle of the rotation axis is not close to $\pi/2$. This may be the reason for no detections of high-quality cycles for stars hotter than the Sun (Fig. 1).

5 CONCLUSIONS

Young rapidly rotating stars are not expected to show sun-like activity cycles. Otherwise, the large-scale stellar dynamos would be an exception among other hydromagnetic instabilities showing turbulence rather than cyclic overstability in a highly supercritical regime.

The upper bound on the rotation period of main-sequence dwarfs showing solar-type magnetic activity (Rengarajan 1984; Metcalfe et al. 2016; van Saders et al. 2016) can be interpreted as the minimum rotation rate for a large-scale stellar dynamos. This rotation rate increases with the effective temperature. Computations with a joint model for differential rotation and dynamo show magnetic cycles for slightly supercritical dynamos in stars of different mass. Hotter stars have shorter cycles in the computations and the hotter stars rotate faster. The observed decrease in cycle duration for faster rotation based on combined statistics of stars of different spectral types can, therefore, be at least partly explained by the cycle dependence on temperature.

[2] Exception from this rule is the rare case of metastability, which is hardly possible to realise with the BL-type dynamo models (Vashishth et al. 2021).

The computations also show larger marginal values of the α-effect for dynamo operation in hotter stars. A larger α demands faster rotation. This may be the reason for the smaller upper bound on the rotation period for hotter stars. The amplitude of magnetic energy in the dynamo model is proportional to the difference between rotation rate and the marginal rate for dynamo (cf. Eq. 21). Stars with similar rotation rates can therefore differ substantially in level of their activity as observed (Reinhold et al. 2020): a small difference in rotation rates does not necessarily mean an equally small super-criticality.

The dynamo computations predict a change in equatorial symmetry of global magnetic fields with temperature. The stars of solar and smaller mass show antisymmetric fields about the equator in the computations. A change to mixed-parity asymmetric fields is predicted for more massive stars. The mixed-parity dynamos can impede observational detection of the activity cycles.

The well-defined activity cycle of subgiant HD 81809 is very interesting and challenging to dynamo theory (see the footnote 1 above). This star exceeds the Sun in mass $M = (1.70 \pm 0.64)M_\odot$ (see table 2 in Egeland 2018). A main-sequence A-star is its probable progenitor. A-stars do not have (sufficiently thick) external convection zones and do not show activity cycles. The convection zone formed when HD 81809 evolved from the main-sequence is probably responsible for its cyclic activity. This example can be informative on the role of convective envelopes for stellar dynamos.

Acknowledgements This work was financially supported by the Ministry of Science and High Education of the Russian Federation.

References

Baliunas, S. L., Donahue, R. A., Soon, W. H., et al. 1995, ApJ, 438, 269 2

Balona, L. A., & Abedigamba, O. P. 2016, MNRAS, 461, 497 2

Barnes, J. R., Collier Cameron, A., Donati, J. F., et al. 2005, MNRAS, 357, L1 2

Barnes, S. A. 2007, ApJ, 669, 1167 2, 9

Boro Saikia, S., Marvin, C. J., Jeffers, S. V., et al. 2018, A&A, 616, A108 3, 4

Brandenburg, A., Saar, S. H., & Turpin, C. R. 1998, ApJ, 498, L51 2

Cameron, R. H., & Schüssler, M. 2016, A&A, 591, A46 7

Cameron, R. H., & Schüssler, M. 2017, ApJ, 843, 111 4

Chandrasekhar, S. 1961, Hydrodynamic and Hydromagnetic Stability (Oxford: Clarendon Press) 4

Charbonneau, P. 2020, LRSP, 17, 4 5

Choudhuri, A. R., Schussler, M., & Dikpati, M. 1995, A&A, 303, L29 5

Collier Cameron, A., & Donati, J. F. 2002, MNRAS, 329, L23 4

Donahue, R. A., Saar, S. H., & Baliunas, S. L. 1996, ApJ, 466, 384 2

Donati, J. F., & Collier Cameron, A. 1997, MNRAS, 291, 1 2

D'Silva, S., & Choudhuri, A. R. 1993, A&A, 272, 621 6

Durney, B. R. 1995, Sol. Phys., 160, 213 5

Durney, B. R., & Latour, J. 1978, Geophysical and Astrophysical Fluid Dynamics, 9, 241 13

Egeland, R. 2018, ApJ, 866, 80 3, 16

Guerrero, G., & de Gouveia Dal Pino, E. M. 2008, A&A, 485, 267 7

Hazra, G., Jiang, J., Karak, B. B., & Kitchatinov, L. 2019, ApJ, 884, 35 2

Høg, E., Fabricius, C., Makarov, V. V., et al. 2000, A&A, 355, L27 3

Jermyn, A. S., Lesaffre, P., Tout, C. A., & Chitre, S. M. 2018, MNRAS, 476, 646 5

Jiang, J., Cameron, R. H., Schmitt, D., & Işık, E. 2013, A&A, 553, A128 5

Jouve, L., Brown, B. P., & Brun, A. S. 2010, A&A, 509, A32 2

Karak, B. B., & Cameron, R. 2016, ApJ, 832, 94 7

Karak, B. B., Kitchatinov, L. L., & Choudhuri, A. R. 2014, ApJ, 791, 59 2

Katsova, M. M., Bondar, N. I., & Livshits, M. A. 2015, Astronomy Reports, 59, 726 10

Kitchatinov, L., & Khlystova, A. 2021, ApJ, 919, 36 15

Kitchatinov, L. L. 2020, ApJ, 893, 131 6

Kitchatinov, L. L., & Nepomnyashchikh, A. A. 2016, Advances in Space Research, 58, 1554 7

Kitchatinov, L. L., & Nepomnyashchikh, A. A. 2017a, Astronomy Letters, 43, 332 5, 6

Kitchatinov, L. L., & Olemskoy, S. V. 2011, MNRAS, 411, 1059 5, 10

Kitchatinov, L. L., & Olemskoy, S. V. 2012, MNRAS, 423, 3344 2, 5

Kitchatinov, L. L., Pipin, V. V., & Ruediger, G. 1994, Astronomische Nachrichten, 315, 157 7

Kitchatinov, L. L., & Rüdiger, G. 1999, A&A, 344, 911 2

Kitchatinov, L., & Nepomnyashchikh, A. 2017b, MNRAS, 470, 3124 4, 5, 7, 8

Kraft, R. P. 1967, ApJ, 150, 551 4

Krause, F., & Rädler, K. H. 1980, Mean-field magnetohydrodynamics and dynamo theory (Oxford: Pergamon Press) 6, 7

Landau, L. D., & Lifshitz, E. M. 1987, Fluid Mechanics. Vol.6 of Course of Theoretical Physics (Oxford: Pergamon Press) 4, 15

Metcalfe, T. S., Egeland, R., & van Saders, J. 2016, ApJ, 826, L2 3, 15

Noyes, R. W., Hartmann, L. W., Baliunas, S. L., Duncan, D. K., & Vaughan, A. H. 1984a, ApJ, 279, 763 4

Noyes, R. W., Weiss, N. O., & Vaughan, A. H. 1984b, ApJ, 287, 769 2

Olspert, N., Lehtinen, J. J., Käpylä, M. J., Pelt, J., & Grigorievskiy, A. 2018, A&A, 619, A6 4

Paxton, B. 2004, PASP, 116, 699 9

Pipin, V. V. 2008, Geophysical and Astrophysical Fluid Dynamics, 102, 21 6

Pipin, V. V. 2021, MNRAS, 502, 2565 2

Pipin, V. V., Sokoloff, D. D., & Usoskin, I. G. 2012, A&A, 542, A26 7

Reinhold, T., Shapiro, A. I., Solanki, S. K., et al. 2020, Science, 368, 518 15, 16

Rengarajan, T. N. 1984, ApJ, 283, L63 3, 15

Rüdiger, G., Kitchatinov, L. L., & Hollerbach, R. 2013, Magnetic Processes in Astrophysics: theory, simulations, experiments (Weinheim: WILEY-VCH) 7

Saar, S. H., & Brandenburg, A. 1999, ApJ, 524, 295 2

Schüssler, M., & Cameron, R. H. 2018, A&A, 618, A89 15

Skumanich, A. 1972, ApJ, 171, 565 2

van Saders, J. L., Ceillier, T., Metcalfe, T. S., et al. 2016, Nature, 529, 181 3, 9, 15

van Saders, J. L., Pinsonneault, M. H., & Barbieri, M. 2019, ApJ, 872, 128 3, 9

VandenBerg, D. A., & Clem, J. L. 2003, AJ, 126, 778 9

Vashishth, V., Karak, B. B., & Kitchatinov, L. 2021, Research in Astronomy and Astrophysics, 21, 266 15

Wilson, O. C. 1968, ApJ, 153, 221 2

Wilson, O. C. 1978, ApJ, 226, 379 2

Zhang, J., Shapiro, A. I., Bi, S., et al. 2020, ApJ, 894, L11 15

Zhang, Z., & Jiang, J. 2022, ApJ, 930, 30 7